Light-Driven Flagella Elucidate the Role of Hook and Cell Body Kinematics in Bundle Formation

S. Bianchi,[1,*] F. Saglimbeni,[1] G. Frangipane,[2] M. C. Cannarsa,[2,3] and R. Di Leonardo[2]
[1]*NANOTEC-CNR, Institute of Nanotechnology, Soft and Living Matter Laboratory, Rome 00185, Italy*
[2]*Department of Physics, "Sapienza" University of Rome, Rome 00185, Italy*
[3]*Department of Biology and Biotechnologies "C. Darwin," "Sapienza" University of Rome, Rome 00185, Italy*

(Received 19 April 2023; accepted 21 August 2023; published 19 September 2023)

Many motile bacteria, such as *Escherichia coli*, swim by rotating multiple flagella. These semiflexible helical filaments are independently actuated by flagellar motors randomly distributed on the surface of the cell body. When all the motors rotate in the same direction, within a fraction of a second, this complex elastohydrodynamic system transforms into a straight swimmer in which all the flagella form a tight bundle propelling the cell forward. Underlying this bundling phenomenon, there are several physical factors, most of which have been analyzed in isolation using theoretical or macroscopic models. Here we report a direct study of bundling dynamics in bacterial cells whose flagellar motors can be switched on and off by light, while fluorescently labeled flagella are observed. Using optical tweezers and microfabrication to constrain cell body kinematics, we found that although translations are not essential for bundling, wobbling plays an important role in achieving a stable configuration of the bundle and body complex. We find that the curved shape of the hook, a flexible joint that transmits motor torque to flagella, strongly affects the vectorial nature of the exchanged torques and must be taken into account to correctly reproduce experimental observations. Finally, we show that once the flagella are aligned, further tightening of the bundle does not lead to an increase in the swimming speed.

DOI: 10.1103/PRXLife.1.013016

I. INTRODUCTION

Peritrichous bacteria, such as *Escherichia coli*, possess multiple flagella positioned almost randomly [1] on the cell body. In their quest for nutrients, *E. coli* cells explore the surroundings alternating between straight trajectories called "runs," in which all the flagella rotate counterclockwise (CCW), and "tumbles," in which at least one flagellum rotates clockwise (CW) and the cells randomly reorient and take a new swim direction [2–4]. During runs, flagella align behind the cell body and eventually can join to form a single flagellar bundle. The physical mechanism that brings the flagella together is still debated. The flagellar hook, which is a 60-nm-long [5] deformable joint connecting the motor and the semirigid flagellum [6], plays a crucial role in the formation of the bundle as it has been found in both theoretical and experimental studies [7,8]. The hooks must be flexible enough to allow the flagella to align in the same direction [7] so that these can deform slightly and wrap in a single bundle. However, it has also been found that, in monoflagellated bacteria, hooks can buckle [9] giving rise to "pseudo-tumbles" usually called "flicks." Similarly, longer hooks in engineered peritrichous bacteria may also buckle and destabilize the flagellar bundle [8]. The role of hydrodynamics in the formation of a tight bundle has also been investigated. It has been shown, experimentally [10–12] and numerically [13–15], that hydrodynamic interactions between two flexible slender bodies, which rotate around their axis and are clamped at one end, drive the filaments to bend and wrap around each other [16]. Following [17], we can refer to this as *direct hydrodynamic interactions* in contrast to *indirect hydrodynamic interactions* given by the cell body translation/rotation. The linear displacement of the cell results in a drag force on the flagella that tends to align them in the opposite direction to the direction of motion [18]. In the frame of reference anchored to the cell body, rotations result in a vortexlike fluid flow whose action combined with elastic response induce the flagella alignment [19]. All these studies focus on isolated aspects, but they do not provide direct experimental evidence of the relative importance of the main factors involved in bundling. Moreover, some important elements such as cell wobbling or the torque transfer from the motor to the flagellum have not been addressed adequately.

Here we study the bundling dynamics of *E. coli* cells whose flagellar motors can be controlled with green light. By expressing the light-driven proton pump proteorhodopsin [20] in our cells, we can use light to control proton motive force in anoxic conditions. Starting from static, spread flagella, we can trigger the rotation of all motors and observe the full development of a tight bundle. To better identify the main mechanisms that bring the flagella together, we can also restrict the degrees of freedom of the cell body by holding it with two optical traps, thus locking translations and wobbling, or by confining it in microfabricated chambers, which prevents translations but allows cell wobbling [21,22]. Moreover, starting from the observation of flagella dynamics

*silvio.bianchi.phys@gmail.com

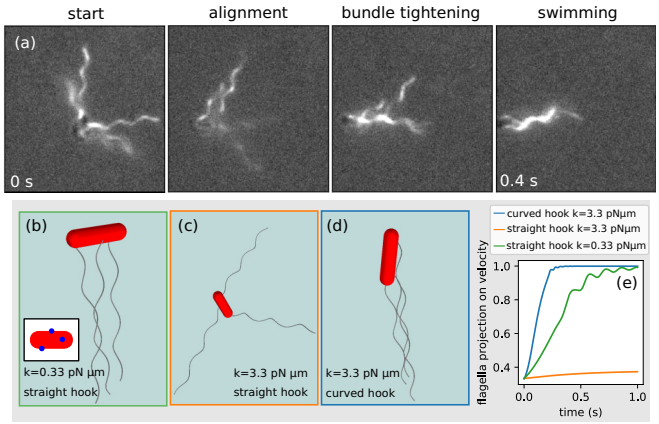

FIG. 1. (a) A cell, which is initially not moving, starts to spin its motors as light is turned on. The flagellar bundle is formed in about 0.4 s. (b)–(d) Numerical simulations of flagella alignment. (b),(c) Curved shape of the hooks is not taken into account: flagellum rest orientation is orthogonal to the cell surface, and applied torque is parallel to the flagellum direction. Flagella attachment points are indicated in the inset in (b) by blue dots (different distributions of attachment points are discussed in Sec. 4 of the Supplemental Material [23]). Motor torque is $T_m = 0.5$ pN µm for all the flagella. (b) If dynamic stiffening of the hook is not considered, the elastic restoring torque per unit angle $k = 0.33$ pN µm is the one measured from dead cells. (c) If the dynamic hook stiffening [24] is taken into account, the elastic constant takes the more realistic value of $k = 3.3$ pN µm. In this situation, the flagella slightly move from their equilibrium position. (d) When the hook's curved shape is taken into account, the torque transferred by the hook is described by Eq. (1). The elastic rest orientation of the flagella forms an angle $\theta_0 = 77^\circ$ with respect to the body normal. The flagella align even for $k = 3.3$ pN µm. (e) Plot of the mean of the flagella projections along the velocity direction (see main text) as a function of time for the simulations shown in (b)–(d).

of cells adhering to the coverglass, we propose a mechanical model of the hook—an almost 90° torque-transmitting joint—and show that its curved structure plays a crucial role in bundle formation. Finally, we analyze a large number of cells to assess the impact of bundle tightness on swimming speed.

II. RESULTS

In the absence of oxygen, we control the proton motive force that powers the flagellar motors with green light thanks to proteorhodopsin. When light is off, the motors stop spinning and flagella spread out in an elastically relaxed state [Fig. 1(a)]. From this initial state, we can trigger a bundle event by quickly turning lights on and following the entire development of a new bundle. We break down this complex process into three main stages. The first one is the "alignment" of isolated flagella along the final bundle direction. During the second stage, "bundle tightening," flagella join together, possibly forming a tight helical propeller where they all spin synchronously. When the bundling is complete, cell body and flagella achieve a stable configuration, and the cell moves in a straight line ("swimming"). In our strain, tumbling is suppressed by deleting the *cheY* gene. It is also worth noting that no hook buckling occurs when the motors resume spinning. Hook buckling occurs in monoflagellated [9] cells and causes the flagellum to rotate about 90° in a short time span of about 10 ms, whereas here we observe flagella aligning smoothly in about 0.4 s.

A. Aligning

After light is turned on, the cell body and the flagella reorient for about 0.5 s to find a common stable axis of rotation (see Supplemental movie 1 [23]). In previously reported numerical models [17,18,25], (i) the motor torque is set to be parallel to the flagellum axis, spinning it around its axis at approximately 100 Hz; (ii) the flagella reorient under the action of an "external" flow due either to translations or rotations of the body; (iii) the hook is taken into account by including an elastic bending response at the flagellum base [17,18,25]. Following [18], where the hook is modeled with a spring with an elastic torque per unit angle k that opposes the reorientation of the flagellum, it turns out that, if the ratio of k to the motor torque T_m is $k/T_m \gtrapprox 0.5$, the flagella do not align and therefore cannot form a bundle. To spin a flagellum, the motor must apply a torque $T_m = \gamma_R^{\parallel}\omega$, where ω is the rotational speed along the flagellum axis and $\gamma_R^{\parallel}$ is the corresponding drag coefficient. We observe that the mean spinning frequency of flagella is about 100 Hz [see Fig. 6(a)]. From the observation Brownian motion of detached flagella, as explained in Sec. 2 of the Supplemental Material [23], we measure the flagellum drag coefficients as a function of the length and interpolate the value of $\gamma_R^{\parallel} = 6.6 \times 10^{-4}$ pN µm s for a flagellum with an average length $2L = 6.7$ µm [see Fig. 6(c)]. Our measurement of the drag coefficients is in fair agreement with previously reported ones obtained with the same method [26]. Using our values for $\gamma_R^{\parallel}$ and ω we obtain $T_m = \gamma_R^{\parallel}\omega \approx 0.5$ pN µm, which is comparable with the previously reported values [27], although it is in the lower end. Observing the Brownian fluctuations of flagella connected to arrested motors, we measure $k = 0.33$ pN µm (see Sec. 1 of the Supplemental Material [23]). This value is not far from those reported in previous studies that are 1.3 pN µm [7] and 0.8 pN µm [24], the latter being computed as EI/H, where $EI = 5 \times 10^{-26}$ N m^2 is the reported value for the bending stiffness of a relaxed hook and $H = 60$ nm is the hook length. Using these numbers, k/T_m happens to be slightly greater than the critical value, but the assumption that the flagella align is still reasonable. However, it has been found that, when the hook is twisted under the action of the motor torque, the former can increase its bending stiffness by a factor between 10 and 20 [24,28], so that a more realistic value for the elastic torque constant would be at least $k \approx 3.3$ pN µm. With this value of k, the ratio k/T_m is more than 10 times larger than the critical value.

If that is the case, how can the flagella reorient? To address this problem we refer to Fig. 2(a), showing two frames of a longer sequence (see Supplemental movie 2 [23]) in which a flagellum, belonging to a cell adhering to the coverglass, spins at approximately 100 Hz while it performs a precession with a period of 1.25 s (0.8 Hz). The transversal drag force bends the flagellum (see Sec. 3 of the Supplemental Material [23]), but here we will neglect this deformation and focus

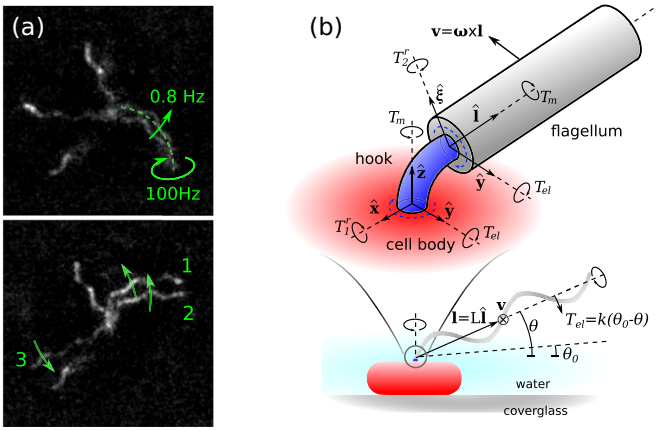

FIG. 2. (a) Two frames from a longer sequence in which a cell adhering to the coverglass spins its flagella. The three numbered flagella both spin around their axis and perform a precession around the motor axis. Flagellum 1 spins at 100 Hz and performs a precession in about 1.25 s (0.8 Hz). (b) A sketch of the cell adhering to the coverglass with a single flagellum of length $2L$. If the hook geometry is taken into account, we obtain a flagellum spinning rapidly around its axis and performing a precession as in (a). This model contributes to explain the reorientation of the flagella, which is the first stage of the bundle formation process.

on the dynamics due to the hook structure. This movement is determined by the transmission of the motor rotation to the flagellum through the hook, which is a universal joint curved by almost 90° at rest [5]. Figure 2(b) shows a sketch of our model that reproduces the observed dynamics. Given the small size of the hook, we approximate its length and its drag coefficients to zero so that all forces/torques acting on it add up to zero. Therefore, the torque $\mathbf{T}$ and the force $\mathbf{f}$ exerted by the motor on the hook are equal, respectively, to the force and the torque exerted by the hook on the flagellum. Placing the origin for torque calculation at the motor base, we can neglect the torque due to force as the hook length is negligible. We consider a flagellum with orientation $\hat{\mathbf{l}}$ laying on the x-z plane as in Fig. 2(b) and write the torque exerted by the motor on the hook, in a most general form, as the sum of three orthogonal components $\mathbf{T} = T_m\hat{\mathbf{z}} + T_{\rm el}\hat{\mathbf{y}} + T_1^r\hat{\mathbf{x}}$. Similarly, we write the torque exerted by the hook on the flagellum as $\mathbf{T} = T_m\hat{\mathbf{l}} + T_{\rm el}\hat{\mathbf{y}} + T_2^r\hat{\boldsymbol{\xi}}$, where $(\hat{\mathbf{l}}, \hat{\mathbf{y}}, \hat{\boldsymbol{\xi}})$ is also an orthogonal triad. The hook acts as a universal joint and transmits the torque $T_m\hat{\mathbf{z}}$ provided by the motor to the flagellum, which experiences a torque $T_m\hat{\mathbf{l}}$. The y component of $\mathbf{T}$ is determined by the elastic bending response of the hook, which restores the flagellum pitch angle θ to its rest position θ_0. We simply express this torque as $T_{\rm el} = k(\theta_0 - \theta)$. Finally, the reaction torques $T_1^r\hat{\mathbf{x}}$ and $T_2^r\hat{\boldsymbol{\xi}}$ are needed to ensure that $T_m\hat{\mathbf{z}} + T_{\rm el}\hat{\mathbf{y}} + T_1^r\hat{\mathbf{x}} = T_m\hat{\mathbf{l}} + T_{\rm el}\hat{\mathbf{y}} + T_2^r\hat{\boldsymbol{\xi}}$. After some manipulations (see Sec. 3 of the Supplemental Material [23]) one can determine the magnitude of $T_{1,2}^r$ and obtain the following simple relation:

$$\mathbf{T} = k(\theta_0 - \theta)\hat{\mathbf{y}} + T_m(\hat{\mathbf{l}} + \hat{\mathbf{z}})/(1 + \hat{\mathbf{l}}\cdot\hat{\mathbf{z}}). \qquad (1)$$

The reaction force $\mathbf{f}$ is not explicit but, using the constraint that the flagellum is attached to the motor, we can uniquely determine the motion of the flagellum. The torque expression in Eq. (1) is substantially different from the one recently proposed in [29] where $\mathbf{T} = T_m\hat{\mathbf{z}}$. In this case, one finds that if the hook is bent at a right angle, the flagellum no longer spins around its axis but only rotates around the motor axis. This is contrary to our observations and the idea that the hook is a universal joint capable of transferring axial torque from the motor axis to the axis of the flagellum, regardless of its orientation.

The details of the model are described in Sec. 3 of the Supplemental Material [23], where we simulate a flagellum of length $2L \approx 6.5$ μm, as in Fig 2(b), attached to a hook with an equilibrium pitch angle of $\theta_0 = 77°$ [5]. We choose a constant [30] motor torque $T_m = 0.42$ pN μm and obtain a flagellum rotation frequency of 100 Hz and a precession frequency of 0.4 Hz; these values compare well with the measured ones, which are about 100 and 0.8 Hz, respectively. Our model also provides a simple analytical solution when the flagellum is horizontal. In this case, the angular velocity projections, on the flagellum axis and to the motor axis, respectively, are $T_m/\gamma_R^{\parallel}$ and $T_m/(\gamma_R^{\perp} + L^2\gamma)$, where $\gamma_R^{\parallel}$ and $\gamma_R^{\perp}$ are the rotational drag coefficients, and $\gamma_{\perp}$ is the linear drag coefficient along a direction perpendicular to the flagellum axis.

We integrate the model described above in simulations with a free cell body with multiple flagella. The cell is initially at rest with its flagella pointing in different directions. The simulation neglects all hydrodynamic interactions and steric repulsion between flagella and between cell body and flagella. Having excluded steric interaction, we also cannot observe the flagella wrapping. Nevertheless, the scope of this simulation is to show that flagella can align in spite of the realistic high value of hook stiffness. Simulation details are described in Sec. 4 of the Supplemental Material [23]. The curved shape of the hooks allows flagella alignment even when considering stiff hooks. In addition to the axial torque along $\hat{\mathbf{l}}$, each flagellum also experiences a torque component along the motor axis $\hat{\mathbf{z}}$ normal to the cell surface [Eq. (1)]. This latter component results in a precession of the flagellar axis around the motor axis. If the hook turn were 90°, this precession would allow the flagella to take the same direction without any elastic deformation. In practice, the hooks bend approximately by 77° [5] and only a small deformation is needed to completely align. Figures 1(b)–1(d) highlight the importance of considering the hook shape. Figures 1(b) and 1(c) show a cell with a "straight" hook where the equilibrium position of the flagellum is normal to the cell body. Also, the torque applied on the flagellum is $\mathbf{T} = T_m\hat{\mathbf{l}}$ (no flagella precession). Using a realistic value for the motor torque $T_m = 0.5$ pN μm, the cell is able to align its flagella only if the hook elasticity k is unrealistically small. In contrast, when the hook is correctly modeled, and using a realistic value of k, flagella realign behind the cell as shown in Fig. 1(d) (see also Supplemental movie 4 [23]). Figure 1(e) plots the flagella alignment as a function of time in the three cases shown in Figs. 1(b)–1(d). For each flagellum, we compute the projection of its axis $\hat{\mathbf{l}}$ along the velocity versor $\hat{\mathbf{v}}$ and then take the average, i.e., $\frac{1}{N}\sum_i \hat{\mathbf{v}}\cdot\hat{\mathbf{l}}$. In simulations, the cell takes about 0.25 s to align its flagella, a value that is comparable with our experimental observations [e.g., see Fig. 1(a)].

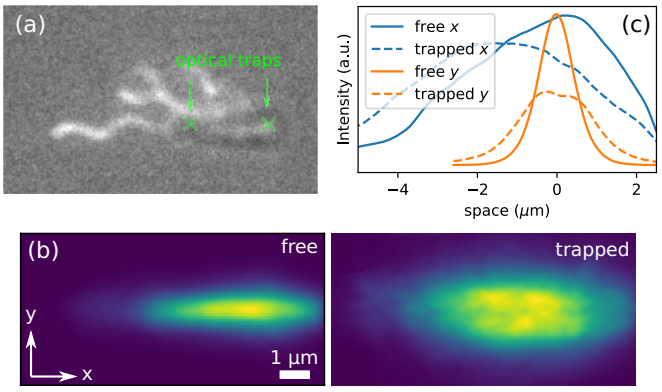

FIG. 3. (a) A cell trapped using optical tweezers is unable to form a tight bundle. In this situation, the cell body is able to rotate only around its main axis (see also Supplemental movie 3 and Sec. 9 of the Supplemental Material [23]). (b) Flagella fluorescence intensity averaged for 24 cells. Each cell is observed both when optically trapped and when it is swimming freely. (c) The flagella averaged intensity is integrated along y and x to compute the profile along x (blue) and y (orange), respectively.

If it is true that the curved structure of the hook is a crucial ingredient for bundle formation, what is the importance of the "external" flow due to cell body motion? To address this point, we observe flagella in a situation in which some of the cell body degrees of freedom are constrained. Figure 3(a) shows a cell being held horizontally by two optical traps. Optical traps prevent the cell from translating and reorienting while rotations along the main body axis are free. We trap 24 cells and compute the average flagella distribution by taking the temporal mean of the fluorescence. The same cells are also observed when swimming freely. The two flagella distributions, reported in Figs. 3(b) and 3(c), are visibly different (see Sec. 9 of the Supplemental Material [23] for details). Holding the cells with traps hinders a tight arrangement of flagella, although in this case it has been found that bundling can be promoted by adding an external upcoming flow [31]. We then suppress the rotation constraints, but still prevent translation of the cell body. We do this by microfabricating the chamber shown in Fig. 4(a). Swimming cells tend to accumulate on surfaces [21,22] and, as they swim on the coverglass, they are guided by a small funnel inside a chamber where they keep swimming for long times. The microchamber is 2 μm wide, therefore cells are able to wobble. Figure 4(b) shows two frames extracted from a sequence where a cell, which is initially idle (light off), forms a bundle as motors are powered on (light is turned on). A small collection of these events is also present in Supplemental movie 5 [23] (in most cases, cells leave the chamber after they restart swimming).

Considering the experimental results described above, we can conclude that, while cell body translations are not essential for flagella alignment, cell wobbling is an important ingredient. To form a tight bundle, both the cell body and flagella must find a common axis of rotation, which does not necessarily coincide with the major axis of the cell body. This can happen only if the cell is free to wobble, which is the case for both a free cell and for a cell in the chamber, but not for an optically trapped cell.

B. Bundle tightening

We record videos of the fluorescently labeled flagella of 45 and 44 cells belonging to the same sample, respectively, swimming freely and inside the chamber. Even for free swimming cells, flagella do not always form a tight diffraction-limited bundle so that in many cases individual flagella cannot be recognized. To quantify the tightness of the bundle, we define a *bundle width* as follows: (i) the bundle center and direction are obtained, respectively, from the first order moment of the intensity and from a major eigenvector of the second order moment matrix; (ii) we center the image on the bundle and rotate it so that

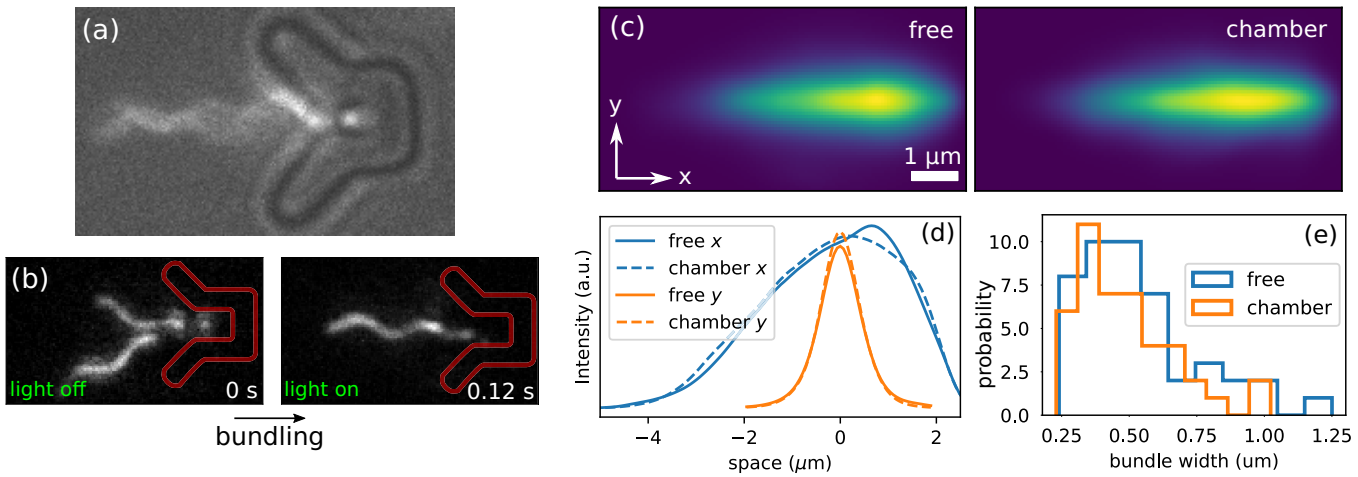

FIG. 4. (a) A cell pushing inside a microfabricated chamber. The chamber is wide enough (2 μm) to allow for wobbling. The V-shaped walls act as a funnel to guide the cell inside the chamber. (b) Two frames extracted from an event in which a cell inside a chamber (drawn in red) forms a bundle. (c) Flagella fluorescence intensity averaged for 24 free swimming cells (left) and 24 cells in chamber (right). The cells are chosen to have a bundle length falling in the interval (4.5,6.5) μm. (d) The flagella averaged intensity is integrated along y and x to compute the profile along x (blue) and y (orange), respectively. (e) Histograms of the bundle width for cells swimming freely and inside the chamber.

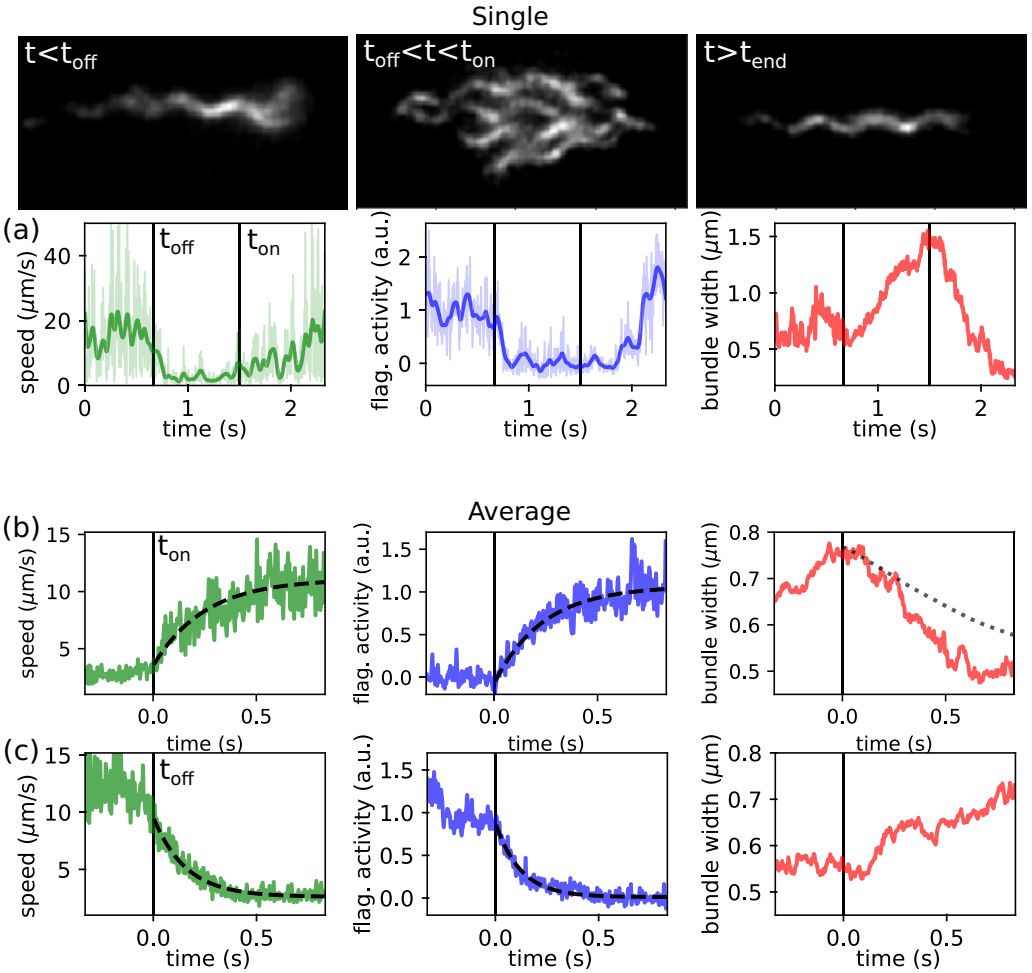

FIG. 5. (a) A sample cell, initially swimming, is de-energized by turning off the light and, after a time lapse of about 1 s in which the bundle breaks, is energized by turning the light back on. The green line plots the cell speed. The blue line plots the flagellar activity, a quantity defined in the main text that is connected to the average flagella rotation speed. Black dashed lines plot fits to exponential functions. The red line plots the bundle width, also defined in the main text. (b),(c) The same quantities averaged for 29 cells. The entire sequence is divided into two parts, one in which cells stop after light is turned off (c), and one in which cells restart by turning the light on (b). The experimental mean bundle width in (b) is compared with a model, plotted as a dotted line, that considers a bundle that tightens only due to cell translations (see Sec. 10 of the Supplemental Material [23]).

the latter is oriented along the x axis [e.g., see Fig. 5(a)]; (iii) for each x we take the slice along y and compute the width as the standard deviation of the intensity along the y axis, i.e., $\sigma(x) = \int dy I(x,y)[y-\bar{y}(x)]^2/\bar{I}(x)$, where $\bar{I}(x) = \int dy I(x,y)$ and $\bar{y}(x) = \int dy I(x,y) y/\bar{I}(x)$; (iv) we compute the total bundle width as $\sigma = \int dx \sigma(x)\bar{I}(x)/\int dx \bar{I}(x)$. The entire procedure is repeated for each frame to compute the time-averaged bundle width. Figure 4(e) shows the histogram of the bundle width for free cells and cells in chamber. The two distributions show no evident difference. A further indication that the bundle shape is unaffected by cell body translations is given by the spatial distribution of flagella: we select 24 cells, both free and in chamber, whose bundle length falls in the interval (4.5,6.5) μm, and we average the fluorescence in time as shown in Fig. 4(c). The integrated profiles along x and y are shown in Fig. 4(d). Again, no significant difference is visible. In the previous section, we showed that flagella can align even when the cell cannot translate; here we also show that translations are not essential to maintain a tight bundle.

For the case of free swimming cells, we will now describe quantitatively the dynamics of bundle formation, starting from a situation in which flagella are almost parallel. To do that, we turn off the light for approximately 1 s and then turn it on again. A few frames of a sample cell are shown in Fig. 5(a). Supplemental movie 6 [23] shows that, as light is turned off, the motors start to slow down and eventually stop completely at different times while the opposite happens when light is turned back on. The time and the order at which the motors stop/start after light is turned off/on is random. We have no explanation for such a random and sudden arrest of the motors. It is known that, when torque provided by the motor drops, stator units disconnect, but the characteristic time for this process is of the order of a few minutes [32]. However, it has been reported [33] that stator units can switch from an active to an inactive "hidden" state without disconnecting completely. The reported characteristic time in this case is about 5 s [33], so that our observations here can be more likely attributed to the latter phenomenology. Figure 5 plots

the linear speed and the bundle width along with a quantity that we called *flagellar activity*, which is connected to the average flagella rotational speed. We defined this quantity since, in most cases, flagella overlap or are partly out of focus so that individual tracking is not feasible. To compute flagellar activity, we start from a cropped image where the bundle is centered and oriented along x. We then perform the following steps: (i) First, the image $I(x, y, t)$ is differentiated in time, i.e., $\partial_t I$. If the flagella do not move, the result is zero, otherwise we have the superposition of two slightly dephased flagella (one positive and one negative). Each slice along x has a signal with periodicity λ (with λ being the flagellum pitch). (ii) We compute the Fourier transform along x, which we indicate by $F[\partial_t I]$, and take the absolute value of the frequency component corresponding to the flagellum pitch $|F[\partial_t I](1/\lambda, y, t)|$. (iii) Finally, we repeat the procedure for each y and compute the average (see Sec. 7 of the Supplemental Material [23] for a detailed description). Plots in Figs. 5(b) and 5(c) show speed, flagellar activity, and bundle width averaged for 29 cells when light is turned on (b) and off (c). Both the motor activity and the speed now show a clear behavior. We fit the velocity curves to the exponential function $v(t) = v_\infty + (v_0 - v_\infty)\exp(-t/\tau)$ and obtain the time constants $\tau_{\text{on}} = 0.30 \pm 0.05$ s and $\tau_{\text{off}} = 0.16 \pm 0.01$ s when light is turned on and off, respectively. We use the same function to fit the activity and obtain $\tau_{\text{on}} = 0.24 \pm 0.02$ s and $\tau_{\text{off}} = 0.120 \pm 0.005$ s.

Experimental [11,12] and theoretical works [14,15] show that two rotating filaments, each clamped at one end, can wrap by direct hydrodynamic interactions alone. For direct hydrodynamic interaction, one can define an adimensional bundling number [13] $\text{Bu} = \xi\omega a^2 L^4/(h_0^2 EI)$ and a timescale $T_b = \xi L^4/EI$, where a and L are the filament radius and length, h_0 is the filament distance, EI is the bending stiffness, and ξ is the drag of the filament per unit length. With a cell thickness of 0.8 μm, we can take as the flagella $h_0 = 0.4$ μm and use realistic numbers for the remaining variables to obtain $\text{Bu} = 0.7$ and $T_b = 1.7$ s. Following [13], for these numbers, the time required to form the bundle is a few seconds. A comparison between this estimate and the experimental behavior of Fig. 5, in which the bundle is formed in 0.5 s, suggests that direct hydrodynamic interactions play a marginal role also when the flagella are close to each other and aligned. We also compare the bundle width track in Fig. 5(b) with a simple model, plotted by a dotted line, in which the bundle tightens only because of the drag force due to the cell linear speed v [18]. The model is described in Sec. 10 of the Supplemental Material [23]. Comparison with the experimental curve also seems to indicate that cell translation may not be the primary mechanism for bundle formation.

C. Swimming

We tracked 279 free swimming cells. For each cell, we compute translational speed, bundle width, bundle rotational frequency, and cell body rotational frequency. The last two can be computed with good accuracy from the frequency spectrum of the image averaged over all pixels. The spectrum shows two distinct peaks, one for the cell body and one for the bundle, from which we extract the rotational frequencies. The distributions of all these quantities are reported in Figs. 6(a)–6(d). The diffraction resolution limit sets a minimum observable bundle width indicated by the orange dashed line in Fig. 6(d). A sample cell with the corresponding bundle width is also shown. The same is done for the median and for a cell in the 99th percentile of the distribution. The cells that join their flagella in a single diffraction limited filament are a minority. It is then a legitimate question to ask whether the bundle tightness gives an advantage in terms of swimming. In the usual simplified picture, we treat cell body and bundle as two separate parts with equal linear speed v and exchanging equal and opposite force/torque,

$$\Gamma v = f, \tag{2}$$

$$\gamma v + c\omega = -f, \tag{3}$$

where f is the force, Γ and γ are the linear drag coefficients of cell body and flagellar bundle, respectively, and c is the rototranslational coupling. The velocity is simply $v = c\omega/(\Gamma + \gamma)$. For a typical 3-μm-long cell, $\Gamma = 0.014$ pN μm^{-1} s (see [34] and Sec. 11 of the Supplemental Material [23]). For a given bundle shape, it is reasonable to assume that the rototranslational coupling scales linearly with the length $c = c'L$ [35]. Our bundle length distribution has a mean value of 6.7 μm and a standard deviation of 1.5 μm. If we roughly estimate γ from a helical-shaped filament, we obtain $\gamma = 0.007 \pm 0.0015$ pN μm^{-1} s (see Secs. 2 and 11 of the Supplemental Material [23]). Variations of the term $\Gamma + \gamma$ due to bundle length are only about 1%, and we therefore write $v \propto c'L\omega$. In Fig. 6(e) we show a scatter plot of v versus $L\omega$; a clear correlation is visible (Pearson coefficient 0.43, P-value 10^{-15}). We divide our cell population into two groups with bundle width higher and smaller, respectively, than the entire population median. We fit the points to a straight line passing through the origin and indicate with the green and red shaded areas in Fig. 6(e) the confidence intervals of the fitted lines. The shaded areas overlap, indicating that there is no significant difference in the swimming efficiency between tight and wide bundles.

We further explore this topic by monitoring the speed-bundle width correlation for each individual cell in time. Even if no tumble is performed, bundles are not completely stationary in time; for instance, a single flagellum can temporarily slip out of the bundle [15]. Starting from all of the 279 cells' time tracks, we obtain the density plot of the bundle width versus the speed shown in Fig. 6(f). For each cell, both of the speed fluctuations are normalized as $(v - \bar{v})/\sigma_v$, where $\bar{v}$ is the time average of v, and σ_v is the standard deviation. Similarly, the normalized bundle width fluctuations are computed, $(w - \bar{w})/\sigma_w$, where w indicates the bundle width. A statistically significant (P-value 10^{-57}) but small correlation is present (Pearson coefficient -0.06) corresponding to a speed increase of only 0.28 μm/s for a bundle tightening of 1 μm [that is more than the range of the width distribution shown in Fig 6(d)]. Further evidence that bundle tightness does not contribute significantly to cell speed is presented in Fig. 6(g), where our experimental data show a negligible correlation between bundle width and speed. Further details of swimming speed and bundle tightness can be found in Sec. 5 of the Supplemental Material [23]. In Sec. 6 of the Supplemental

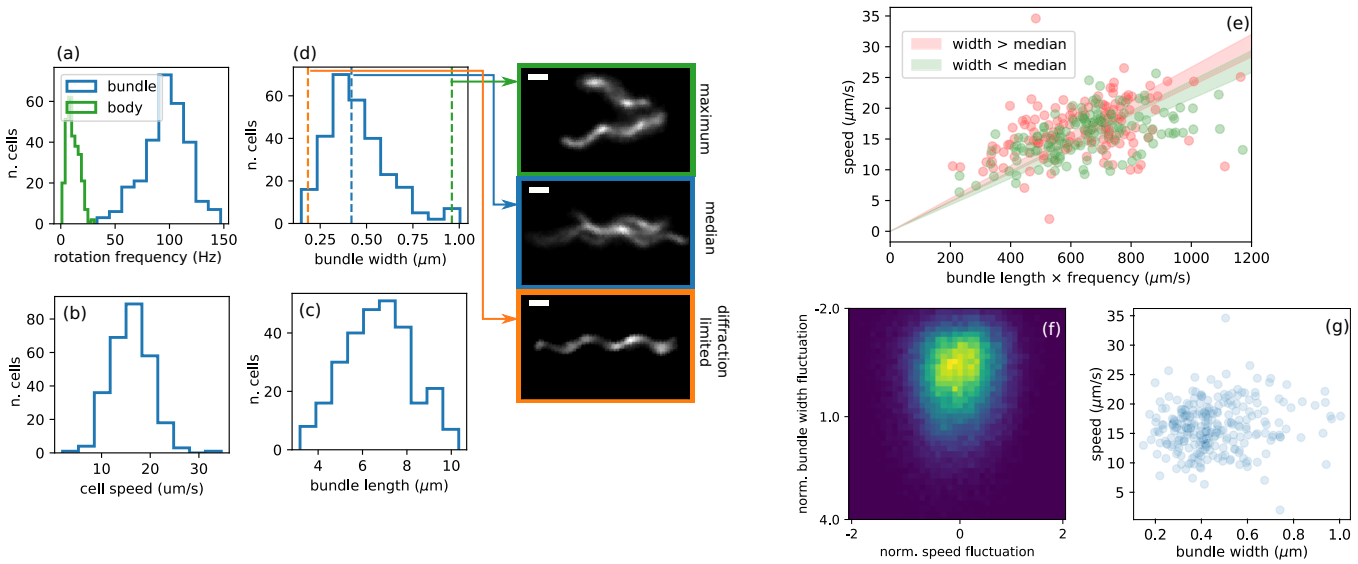

FIG. 6. (a)–(d) Distribution of some measurable quantities for free swimming cells. (a) Cell body and flagellar bundle rotational frequency for cell speed (b), bundle length (c), and bundle width (d). A sample frame of a bundle whose width is close to the diffraction limit value is shown along with two others whose widths are near, respectively, the median and the maximum of the distribution. Scale bars are 1 μm. (e) Swimming speed as a function of the product of the bundle length and the bundle frequency. We divide the sample into two groups of cells with bundle widths above and below the median. Points can be fitted to a straight line passing through the origin. The angular coefficients, which are strictly connected to the bundle rototranslational coupling per unit length, do not differ significantly. (f) Density plot built from the fluctuations in time of the speed and of the bundle width for all 279 cells. (g) Swimming speed as a function of bundle width.

Material [23], we also simulate a cell with two flagella and compute the linear speed as a function of the flagella separation. Simulations of deformable flagella predict that these can synchronize [36,37] and form an almost perfect bundle [14,38], but only a small enhancement in the swimming efficiency is predicted [14]. In our experiments, we find only a marginal speed increase even when the separation of the two flagella is below the diffraction limit.

This last result suggests that the purpose of having multiple flagella is that cells can always perform a run-and-tumble motion. The chemotactic mechanism of monoflagellated bacteria relies on hook buckling [9], and, below a threshold ion motive force, the motor thrust is too low to buckle the hook [9]. On the contrary, multiflagellated bacteria such as *E. coli*, which reverses the spinning direction of one flagellum to perform a tumble, can always perform their run-and-tumble motion even at low proton motive force.

III. CONCLUSIONS

Fluorescent staining of bacterial flagella revealed that *E. coli* swims smoothly when flagella bundle together in a tight propeller [3]. However, the physical mechanism that drives bundle formation could only be explored by observing transient and partial bundle disruptions caused by tumbling. Here we use light-activated flagellar motors to study bundling dynamics starting from a fully relaxed static state. The curved shape of the hook is essential to account for flagellar dynamics during bundle formation. The resulting precession movement allows an initial alignment of the flagella, enabling the bundle to be formed even considering the stiffening of the rotating hook. By combining fluorescence imaging with optical tweezers and microfabrication we found that, among cell body degrees of freedom, wobbling appears to be a necessary element for the formation of tight bundles. Finally, our experiments show that bundle tightness has a negligible impact on swimming speed. Future work may explore the role of hook in the bundling dynamics of individual light-activated cells using engineered strains with straight hooks [7] or with variable lengths [8] and rigidity [7,39]. In addition, the role of oscillation could be further investigated by using microchambers of different shapes that impose different degrees of restriction on wobbling.

ACKNOWLEDGMENT

This project has received funding from the European Research Council (ERC) under the European Union's Horizon 2020 research and innovation programme (Grant Agreement No. 834615).

APPENDIX: MATERIALS AND METHODS

1. Cell growth and sample preparation

For all experiments, we used a smooth swimmer photokinetic strain with stainable flagella. The strain is a derivative strain of HCB1737 Δ*cheY* [40], a smooth swimmer that expresses a modified flagellin (fliC) bearing a specific cysteine-for-serine substitution (S219C) that allows filaments to be specifically labeled with the maleimide fluorescent dye Alexa Fluor 680 C_2 Maleimide (A-20344; Life Technologies, Carlsbad, CA). To implement photokinesis, we followed the same procedure of [41], deleting the atp operon and transforming the strain with a plasmid expressing the protein proteorhodopsin, which acts as a light inducible proton pump.

Cells were streaked on a Petri dish containing 1.5% of agar and Lysogeny Broth (LB, 1% tryptone, 0.5% NaCl, 0.5% Yeast extract). A single colony was inoculated into LB and grown overnight at 30 °C with 200 rpm rotation. The saturated culture was then diluted 1:100 (50 μL in 5 mL) into fresh tryptone broth (1% tryptone, 0.5% NaCl) and grown for 4 h at 30 °C with 200 rpm rotation. All the growth media are supplemented with 100 μg/mL of ampicillin. Then all-trans-retinal (20 μM) and l-arabinose (1 mM) were added to ensure expression and proper folding of proteorhodopsin in the membrane. The growth medium was washed after 1 h of induction by centrifugation at 1300×g for 5 min at room temperature for three times, and cells were resuspended in 500 μL of motility buffer (KH_2PO_4 and K_2HPO_4, pH 7.0, 100 mM EDTA, and 10 mM of glucose). The labeling procedure was performed as described in [42]. 1 mg of dye was dissolved in 300 μL water by vortexing. The solution was aliquoted in 20 μL samples and stored at −80 °C. After washing the growth medium, the 500 μL of bacterial suspension was gently mixed with 10 μL of the dissolved dye at room temperature and agitated (100 rpm) in the dark for 90 min. Finally, the culture was washed from the dye and resuspended in a minimal motility buffer composed of potassium phosphate 100 mM (KH_2PO_4 and K_2HPO_4, pH 7.0), 100 mM EDTA and 10 mM of glucose, 0.02% Tween 20, and an oxygen scavenging system [43,44]. The cells were washed six times, through centrifugation as before, to remove the unreacted dye from the medium.

2. Imaging of fluorescently labeled flagella

Fluorescent flagella were imaged in epifluorescence by illuminating them with a red laser (Integrated Optics, MatchBox 660 nm 0660L-13A-NI-PT-NF). Laser is focused on the back-focal plane of the objective (Nikon Plan Apo 100X NA 1.4) to produce a collimated beam of about 60 μm in diameter to excite the fluorophores. Stroboscopic illumination is obtained via an acousto-optic modulator (NEC, A-O Modulator Mod. OD-8813A) in order to reduce bleaching of the fluorophore and blurring of the images. We acquired images at 300 frames per second, synchronizing the camera (Hamamatsu Orca 4.0) with the acousto-optic modulator, employing duty-cycles varying from 0.05 to 0.15 depending on fluorescence intensity. Fluorescence is excited and recorded using the fluorescence filter set Cy5.5 from Edmund Optics. In most acquisitions, a weak bright field illumination is provided by a red LED from above to show the cell bodies alongside the fluorescent flagella. Finally, to energize the photokinetic bacteria, we use a green LED (Thorlabs, M530L4) with an emission peak at 530 nm, passing through the objective.

[1] L. Ping, The asymmetric flagellar distribution and motility of *Escherichia coli*, J. Mol. Biol. **397**, 906 (2010).

[2] H. C. Berg, *E. coli in Motion* (Springer, New York, 2004).

[3] L. Turner, W. S. Ryu, and H. C. Berg, Real-time imaging of fluorescent flagellar filaments, J. Bacteriol. **182**, 2793 (2000).

[4] L. Turner, L. Ping, M. Neubauer, and H. C. Berg, Visualizing flagella while tracking bacteria, Biophys. J. **111**, 630 (2016).

[5] A. Sen, R. K. Nandy, and A. N. Ghosh, Elasticity of flagellar hooks, J. Electron Microscopy **53**, 305 (2004).

[6] N. C. Darnton and H. C. Berg, Force-extension measurements on bacterial flagella: triggering polymorphic transformations, Biophys. J. **92**, 2230 (2007).

[7] M. T. Brown, B. C. Steel, C. Silvestrin, D. A. Wilkinson, N. J. Delalez, C. N. Lumb, B. Obara, J. P. Armitage, and R. M. Berry, Flagellar hook flexibility is essential for bundle formation in swimming *Escherichia coli* cells, J. Bacteriol. **194**, 3495 (2012).

[8] I. Spöring, V. A. Martinez, C. Hotz, J. Schwarz-Linek, K. L. Grady, J. M. Nava-Sedeño, T. Vissers, H. M. Singer, M. Rohde, C. Bourquin *et al.*, Hook length of the bacterial flagellum is optimized for maximal stability of the flagellar bundle, PLoS Biol. **16**, e2006989 (2018).

[9] K. Son, J. S. Guasto, and R. Stocker, Bacteria can exploit a flagellar buckling instability to change direction, Nat. Phys. **9**, 494 (2013).

[10] R. M. Macnab, Bacterial flagella rotating in bundles: a study in helical geometry, Proc. Natl. Acad. Sci. (USA) **74**, 221 (1977).

[11] M. Kim, J. C. Bird, A. J. Van Parys, K. S. Breuer, and T. R. Powers, A macroscopic scale model of bacterial flagellar bundling, Proc. Natl. Acad. Sci. (USA) **100**, 15481 (2003).

[12] M. J. Kim, M. J. Kim, J. Bird, J. Park, T. Powers, K. S. Breuer *et al.*, Particle image velocimetry experiments on a macro-scale model for bacterial flagellar bundling, Exp. Fluids **37**, 782 (2004).

[13] Y. Man, W. Page, R. J. Poole, and E. Lauga, Bundling of elastic filaments induced by hydrodynamic interactions, Phys. Rev. Fluids **2**, 123101 (2017).

[14] S. Y. Reigh, R. G. Winkler, and G. Gompper, Synchronization and bundling of anchored bacterial flagella, Soft Matter **8**, 4363 (2012).

[15] S. Y. Reigh, R. G. Winkler, and G. Gompper, Synchronization, slippage, and unbundling of driven helical flagella, PLoS One **8**, e70868 (2013).

[16] T. C. Adhyapak and H. Stark, Zipping and entanglement in flagellar bundle of *E. coli*: Role of motile cell body, Phys. Rev. E **92**, 052701 (2015).

[17] A. Chamolly and E. Lauga, Direct versus indirect hydrodynamic interactions during bundle formation of bacterial flagella, Phys. Rev. Fluids **5**, 123102 (2020).

[18] E. E. Riley, D. Das, and E. Lauga, Swimming of peritrichous bacteria is enabled by an elastohydrodynamic instability, Sci. Rep. **8**, 10728 (2018).

[19] T. R. Powers, Role of body rotation in bacterial flagellar bundling, Phys. Rev. E **65**, 040903(R) (2002).

[20] O. Béja, L. Aravind, E. V. Koonin, M. T. Suzuki, A. Hadd, L. P. Nguyen, S. B. Jovanovich, C. M. Gates, R. A. Feldman, J. L. Spudich *et al.*, Bacterial rhodopsin: evidence for a new type of phototrophy in the sea, Science **289**, 1902 (2000).

[21] S. Bianchi, F. Saglimbeni, and R. Di Leonardo, Holographic Imaging Reveals the Mechanism of Wall Entrapment in Swimming Bacteria, Phys. Rev. X **7**, 011010 (2017).

[22] S. Bianchi, F. Saglimbeni, G. Frangipane, D. Dell'Arciprete, and R. Di Leonardo, 3d dynamics of bacteria wall entrapment at a water–air interface, Soft Matter **15**, 3397 (2019).

[23] See Supplemental Material at http://link.aps.org/supplemental/10.1103/PRXLife.1.013016 for additional information and movies.

[24] A. L. Nord, A. Biquet-Bisquert, M. Abkarian, T. Pigaglio, F. Seduk, A. Magalon, and F. Pedaci, Dynamic stiffening of the flagellar hook, Nat. Commun. **13**, 2925 (2022).

[25] T. Eisenstecken, J. Hu, and R. G. Winkler, Bacterial swarmer cells in confinement: a mesoscale hydrodynamic simulation study, Soft Matter **12**, 8316 (2016).

[26] F. Djutanta, P. T. Brown, B. Nainggolan, A. Coullomb, S. Radhakrishnan, J. Sentosa, B. Yurke, R. F. Hariadi, and D. P. Shepherd, Decoding the hydrodynamic properties of microscale helical propellers from brownian fluctuations, Proc. Natl. Acad. Sci. (USA) **120**, e2220033120 (2023).

[27] D. Das and E. Lauga, Computing the motor torque of *Escherichia coli*, Soft Matter **14**, 5955 (2018).

[28] X. Zhang, C. Zhang, R. Zhang, and J. Yuan, Differential Bending Stiffness of the Bacterial Flagellar Hook under Counterclockwise and Clockwise Rotations, Phys. Rev. Lett. **130**, 138401 (2023).

[29] Y. Shimogonya, Y. Sawano, H. Wakebe, Y. Inoue, A. Ishijima, and T. Ishikawa, Torque-induced precession of bacterial flagella, Sci. Rep. **5**, 18488 (2015).

[30] X. Chen and H. C. Berg, Torque-speed relationship of the flagellar rotary motor of *Escherichia coli*, Biophys. J. **78**, 1036 (2000).

[31] G. Liu, Z. Liu, L. Zhu, R. Zhang, and J. Yuan, Upcoming flow promotes the bundle formation of bacterial flagella, Biophys. J. **120**, 4391 (2021).

[32] A. L. Nord, E. Gachon, R. Perez-Carrasco, J. A. Nirody, A. Barducci, R. M. Berry, and F. Pedaci, Catch bond drives stator mechanosensitivity in the bacterial flagellar motor, Proc. Natl. Acad. Sci. (USA) **114**, 12952 (2017).

[33] H. Shi, S. Ma, R. Zhang, and J. Yuan, A hidden state in the turnover of a functioning membrane protein complex, Sci. Adv. **5**, eaau6885 (2019).

[34] M. Reichert, Hydrodynamic Interactions in Colloidal and Biological Systems, Ph.D. thesis, Universitat Konstanz, Konstanz (2006).

[35] S. Bianchi, V. Carmona Sosa, G. Vizsnyiczai, and R. Di Leonardo, Brownian fluctuations and hydrodynamics of a microhelix near a solid wall, Sci. Rep. **10**, 4609 (2020).

[36] P. J. A. Janssen and M. D. Graham, Coexistence of tight and loose bundled states in a model of bacterial flagellar dynamics, Phys. Rev. E **84**, 011910 (2011).

[37] M. Tătulea-Codrean and E. Lauga, Elastohydrodynamic Synchronization of Rotating Bacterial Flagella, Phys. Rev. Lett. **128**, 208101 (2022).

[38] F. T. M. Nguyen and M. D. Graham, Impacts of multiflagellarity on stability and speed of bacterial locomotion, Phys. Rev. E **98**, 042419 (2018).

[39] T. Fujii, H. Matsunami, Y. Inoue, and K. Namba, Evidence for the hook supercoiling mechanism of the bacterial flagellum, Biophys. Physicobiol. **15**, 28 (2018).

[40] S. Bianchi, F. Saglimbeni, G. Frangipane, and R. Di Leonardo, Flagellar elasticity and the multiple swimming modes of interfacial bacteria, Phys. Rev. Res. **4**, L022044 (2022).

[41] H. Massana-Cid, C. Maggi, G. Frangipane, and R. Di Leonardo, Rectification and confinement of photokinetic bacteria in an optical feedback loop, Nat. Commun. **13**, 2740 (2022).

[42] P. J. Mears, S. Koirala, C. V. Rao, I. Golding, and Y. R. Chemla, *Escherichia coli* swimming is robust against variations in flagellar number, eLife **3**, e01916 (2014).

[43] K. C. Neuman, E. H. Chadd, G. F. Liou, K. Bergman, and S. M. Block, Characterization of photodamage to *Escherichia coli* in optical traps, Biophys. J. **77**, 2856 (1999).

[44] T. L. Min, P. J. Mears, L. M. Chubiz, C. V. Rao, I. Golding, and Y. R. Chemla, High-resolution, long-term characterization of bacterial motility using optical tweezers, Nat. Methods **6**, 831 (2009).